

## Molecular Physics

An International Journal at the Interface Between Chemistry and Physics

ISSN: 0026-8976 (Print) 1362-3028 (Online) Journal homepage: <http://www.tandfonline.com/loi/tmph20>

# Phase behaviour of colloids suspended in a near-critical solvent: a mean-field approach

John R. Edison, Simone Belli, Robert Evans, René van Roij & Marjolein Dijkstra

To cite this article: John R. Edison, Simone Belli, Robert Evans, René van Roij & Marjolein Dijkstra (2015) Phase behaviour of colloids suspended in a near-critical solvent: a mean-field approach, Molecular Physics, 113:17-18, 2546-2555, DOI: [10.1080/00268976.2015.1031842](https://doi.org/10.1080/00268976.2015.1031842)

To link to this article: <http://dx.doi.org/10.1080/00268976.2015.1031842>



Published online: 15 Apr 2015.



Submit your article to this journal [↗](#)



Article views: 92



View related articles [↗](#)



View Crossmark data [↗](#)

Full Terms & Conditions of access and use can be found at  
<http://www.tandfonline.com/action/journalInformation?journalCode=tmph20>

## INVITED ARTICLE

## Phase behaviour of colloids suspended in a near-critical solvent: a mean-field approach

John R. Edison<sup>a</sup>, Simone Belli<sup>b</sup>, Robert Evans<sup>c</sup>, René van Roij<sup>b</sup> and Marjolein Dijkstra<sup>a,\*</sup><sup>a</sup>*Soft Condensed Matter, Debye Institute for NanoMaterials Science, Utrecht University, Utrecht, The Netherlands;* <sup>b</sup>*Institute for Theoretical Physics, Utrecht University, Utrecht, The Netherlands;* <sup>c</sup>*H.H. Wills Physics Laboratory, University of Bristol, Bristol, United Kingdom*

(Received 15 February 2015; accepted 16 March 2015)

Colloids suspended in a binary solvent may, under suitable thermodynamic conditions, experience a wide variety of solvent-mediated interactions that can lead to colloidal phase transitions and aggregation phenomena. We present a simple mean-field theory, based on free-volume arguments, that describes the phase behaviour of colloids suspended in a near-critical binary solvent. The theory predicts rich phase behaviour: we find colloidal gas, liquid and crystal phases, a colloidal gas–liquid critical line and a colloidal solid–solid critical line. We compare our results with those of our recent simulation study of the same model in two dimensions. Our simple theory accounts for the main features of the phase diagrams found in simulations and sheds new light on the origin of colloidal aggregation lines in near-critical solvents.

## 1. Introduction

Understanding how solvent-mediated (SM) interactions between colloidal particles can dictate aggregation and colloidal self-assembly is a key goal for colloid science. An important situation is when the solvent is close to its critical point. Then the SM interaction between two colloidal particles becomes long-ranged; it is governed by the (diverging) correlation length  $\xi$  of the solvent. In this paper we present a simple theory aimed at understanding colloidal phase behaviour and aggregation for a lattice model of a dense suspension of colloidal particles in a binary solvent that is near its critical point.

Consider a binary AB solvent that displays a de-mixing phase transition below a critical point at temperature  $T_c$  and composition  $x_c$ . Colloidal particles are suspended in this solvent and we suppose these prefer solvent species B, i.e. there is preferential adsorption of B. Depending on the temperature  $T$  and composition  $x$  of the solvent, a wide variety of adsorption and wetting related phenomena can occur at the surface of a colloidal particle. In the near-critical region of the solvent  $T \rightarrow T_c$ ,  $x \rightarrow x_c$  films of the preferred species will adsorb on a single colloid, up to a length scale given by the correlation length of the solvent, e.g. [1]. Sufficiently close to the solvent critical de-mixing point the thickness of the adsorbed films diverges in the same fashion as the bulk correlation length, according to the scaling law  $\xi \sim |\tau|^{-\nu}$ , with  $\tau = (T - T_c)/T_c$ . It follows that two colloids suspended in the same, near-critical, solvent will experience a SM interaction that can extend to very long distances. Fisher and de Gennes made this prediction three decades ago [2] and argued that the SM interaction should display

universal scaling properties with scaling functions depending on the ratio of the particle separation to the correlation length. In recent years direct experimental measurements were performed [3,4] of the force between a colloidal particle and a flat wall for a near-critical (water–lutidine, WL) binary solvent mixture. The near-critical SM interactions are often referred to as critical Casimir interactions, making analogy with the confining effects of quantum fluctuations of the electromagnetic field [5]. These critical ‘Casimir’ SM interactions depend on the preferential adsorption of the solvent on the two colloids. For example, identical colloidal particles will experience SM attraction whereas two different colloids, one preferring species B and the other A, will exhibit repulsion and the scaling functions are different. Theoretical studies of critical Casimir interactions begin by considering solvent confinement between two planar walls and determining the scaling behaviour of the SM force for various universality classes [5,6]. The well-known Derjaguin approximation is then employed to convert results from the planar case to those appropriate to the force between two spherical particles. It is important to recognise that even at supercritical solvent state points that are away from the critical scaling regime the SM interactions can be strong and might influence phase behaviour for a dense suspension of colloids.

Turning now to the subcritical region of the solvent  $T < T_c$ , strong preferential adsorption can lead to bridging transitions [7] between two identical colloidal particles (equivalent to a rounded capillary condensation transition of a binary mixture between two identical planar substrates). This scenario occurs if the bulk solvent phase is rich in A but

\*Corresponding author. Email: [m.dijkstra1@uu.nl](mailto:m.dijkstra1@uu.nl)

the colloids prefer the phase rich in B, leading to a capillary bridge of the latter. This leads to an SM interaction between the colloids that is strongly attractive [8–10]. We emphasise such transitions occur in the A-rich region of the phase diagram. Rounded pre-wetting transitions can also manifest themselves in the effective SM interaction between colloidal particles [11,12]. Unlike the critical Casimir SM interactions these subcritical interactions, driven by considerations of wetting, are non-universal and depend in a detailed way on the nature of the local interactions between a colloid and the binary solvent. An important feature of all SM interactions is their sensitivity to the temperature and composition of the solvent. This raises prospects of performing colloidal self-assembly in a reversible and *in situ* manner by manipulating the temperature thereby tuning the effective interactions.

Our present study focuses on a dense suspension of colloids in a near-critical binary solvent rather than on a very dilute system where only interactions between a pair of colloids are relevant. That is, we are concerned with the situation where not only pairwise but also many-body SM interactions between colloids might come to the fore.

There have been several experimental investigations of near-critical colloidal aggregation or self-assembly, e.g. [13–16]; for a recent study see [17]. In 1985 Beysens and Estève [13] made the first observation of reversible colloidal aggregation in their pioneering investigation of a system of silica colloids suspended in a WL mixture. The WL solvent exhibits a de-mixing phase transition above the (lower) critical temperature  $T_c = 34^\circ\text{C}$  and the critical lutidine mass fraction  $x_c = 0.286$ . The silica colloids had an inherent preference for adsorption of lutidine over water. A suspension of colloids, initially at  $T < T_c$  and  $x < x_c$ , exhibited aggregation upon heating to a well-defined temperature  $T_a$ . The aggregation temperature depended on the solvent composition  $x$ , and an aggregation line could be determined, below the binodal of the WL mixture, i.e. in the one-phase region of the solvent. Beysens and Estève noted that aggregation was observed only in the water-rich region ( $x < x_c$ ) of the solvent. In their original paper Beysens and Estève identified the aggregation line with a pre-wetting line linked with strong adsorption of the wetting phase (L) on the silica colloids. However, unlike pre-wetting at a macroscopic substrate, the aggregation line extended to below the critical temperature into the one-phase region of the solvent. In an article published in 1999, Beysens and Narayanan [18] review several experimental studies and suggest that the scenario found in the WL studies is rather general: aggregation is found near the binodal of the solvent phase not preferred by the colloids. Recently there has been a resurgence of interest in studying a dense suspension of colloids in a near-critical binary solvent [17]. In particular, using confocal microscopy, Schall and co-workers have made real-space measurements of the SM colloidal aggregation process [16,17].

Motivated by both the early and recent experiments we performed computer simulations [19] for a simple two-dimensional (2D) lattice based model, i.e. we investigated the phase behaviour of hard-disk colloids suspended in a near-critical binary lattice gas (AB) solvent. Our simulation results revealed: (1) the presence of gas–liquid (G-L) and gas–crystal (G-X) coexistence at state points both close to and far from the criticality of the solvent reservoir. (2) The critical point of the ternary mixture is shifted from that of the solvent reservoir upon adding a small fraction of colloids. (3) Two-body SM interactions, calculated in the dilute limit, are not sufficient to account accurately for the critical point shift, and (4) the phase separation is driven by preferential adsorption of one species of solvent on the (model) colloid. Our results pertained to the supercritical (one-phase) region of the solvent. The richness of the simulation phase diagrams led us to enquire whether a simple mean-field theory could describe the overall features of the phase behaviour that we observe. Such a theory might then form the basis for a description of the continuum ternary fluid mixture.

We are not the first to attempt to develop a theory. There have been several attempts to account for the observation of reversible colloidal aggregation in near-critical solvents. The review [18] summarises the early ones and it would not be appropriate to re-visit all of these. The work of [20,21] focused on the situation where the solvent reservoir is subcritical and described the implications of wetting and capillary bridging transitions for the phase behaviour of model colloidal suspensions. Earlier Sluckin [22] had argued that aggregation should be viewed as phase separation in a ternary system. The same viewpoint was adopted in [14]. More recently, Mohry *et al.* [23–25] studied the structure, phase behaviour and aggregation of model colloids immersed in a near-critical solvent using an effective one-component description. The solvent is assumed to give rise to pairwise SM interactions between the colloidal particles which depend on temperature and solvent composition. The attractive portions of the pair potentials are extracted from Monte Carlo simulations, e.g. [6] of the critical Casimir scaling functions using the Derjaguin approximation. Schall and co-workers [17,26] adopt a similar standpoint, except the SM pair potentials are extracted from experiment. Such an approach can be expected to be reliable for very dilute suspensions where many-body interactions might not be very important. However, it is not clear a priori that a pairwise description of the SM interactions is sufficient to capture all the features of phase behaviour that might occur in dense suspensions. Moreover, when the correlation length of the solvent is large, perhaps comparable with the size of the colloid, one expects many-body effects to be important.

The theory we develop and implement here is not based on an effective pair potential description. Rather it is in the spirit of some of the earlier approaches. We consider the

lattice model treated in our simulations [19] and mentioned above. Using free-volume arguments we write down an approximation for the Helmholtz free energy of the AB solvent that lives on the lattice sites not occupied by colloidal disks in 2D or spheres in 3D. Our theory is arguably the simplest mean-field treatment of a ternary mixture where one of the species is much larger in size than the other two and where this large species has an inherent preference to adsorb one of the two smaller species. In Section 2 we describe our lattice model. The mean-field theory is described in Section 3 and in Section 4 we present results for the phase diagrams. As in our simulation study [19] we focus on situations where the solvent reservoir is supercritical. Finally in Section 5 we summarise our results and discuss their implications for colloidal aggregation.

## 2. Model

We describe the ternary system using a simple lattice model. Colloids (C) are discretised hard particles (disks/spheres) with radius  $R$ , that can undergo Brownian motion in a binary lattice solvent (AB). The Hamiltonian  $H_C$  describing the bare colloids is simple. The potential energy is zero for non-overlapping configurations, and infinite if any pair of hard colloids overlaps. Every lattice site  $i$  has an occupancy number  $n_i = 1$  if it is occupied by a colloidal disk, and  $n_i = 0$  if it is available for an A or a B solvent molecule. For every solvent occupied site we assign an occupancy number  $s_i = -1$  if it is occupied by A, and  $s_i = 1$  for B. We consider only nearest neighbour interactions, and assign an energy penalty  $\epsilon/2 > 0$  for every nearest neighbour AB pair in order to drive AB de-mixing at sufficiently low temperatures. We impose an energy gain of  $-\alpha\epsilon/2$  with  $\alpha \geq 0$  for every BC pair to mimic preferential adsorption of solvent species B on the colloid (C) surfaces. The total Hamiltonian of the ternary ABC system is given by

$$H = H_C + \frac{\epsilon}{4} \sum_{(i,j)} (1 - s_i s_j)(1 - n_i)(1 - n_j) - \frac{\alpha\epsilon}{4} \sum_{(i,j)} n_i(1 + s_j)(1 - n_j) \quad (1)$$

where the summation runs over the set of distinct nearest neighbour pairs  $ij$ . This is the model that was treated by Monte Carlo simulations in [19].

## 3. Theory

The free energy of the ternary ABC model is calculated within a simple mean-field approximation. For a lattice consisting of  $M$  sites, the colloids occupy a fraction  $\eta$  of these, and the remaining free ‘volume’  $M(1 - \eta)$  is filled by the AB binary solvent. The fraction of sites occupied by B is denoted by  $x$ , so that the fraction of sites occupied by A is

$1 - \eta - x$ . The mean-field Helmholtz free energy of the system can be written as

$$F_{\text{MF}}(N_c, M, T, x) = F_C(N_c, M, T) + (1 - \eta)F_{\text{AB}}(N_s, M, T) + N_c U_{\text{BC}} \quad (2)$$

where  $N_c$  is the number of colloidal particles and  $N_s$  is the number of molecules of solvent species B. Note that due to the incompressible lattice nature of the solvent,  $N_c$  and  $N_s$  suffice to describe uniquely the number of particles of each species present in the system. Thus the ternary system is equivalent to a binary system. In Equation (2) the first term  $F_C(N_c, M, T)$  is the pure-colloid contribution.  $F_{\text{AB}}(N_s, M, T)$  is the mean-field free energy of the binary AB mixture in the free space in between the colloids (with fractions  $1 - \hat{x}$  and  $\hat{x} \equiv x/(1 - \eta)$  of A and B, respectively).  $U_{\text{BC}}$  is the average adsorption energy of the B solvent on the colloid surface. This yields, up to irrelevant additive constants,

$$F_{\text{MF}}(N_c, M, T, x) = F_c(N_c, M, T) - N_c z_{cs} \alpha \epsilon \hat{x} + (1 - \eta)M(k_B T [\hat{x} \ln \hat{x} + (1 - \hat{x}) \ln(1 - \hat{x})] + \frac{z_{ss}}{2} \epsilon \hat{x}(1 - \hat{x})) \quad (3)$$

where  $F_c$  is the Helmholtz free energy of a system of hard disks (spheres),  $\eta$  is the packing fraction of the hard disks,  $T$  is the temperature,  $k_B$  is the Boltzmann constant,  $z_{ss}$  is the coordination number of the lattice (in 2D for a square lattice  $z_{ss} = 4$ ),  $z_{cs}$  is the total number of nearest neighbours for a colloid of radius  $R$  and  $\hat{x}$  is the fraction of the solvent in the free volume  $(1 - \eta)M$ . Note that the overall solvent composition  $x = N_s/M$ . The free energy per site can be written as

$$\frac{F_{\text{MF}}(\eta, T, x)}{M} = \frac{F_c(\eta, T)}{M} - \frac{\eta}{v_c} z_{cs} \alpha \epsilon \frac{x}{1 - \eta} + k_B T \left[ x \ln \frac{x}{1 - \eta} + (1 - x - \eta) \times \ln \left( \frac{1 - x - \eta}{1 - \eta} \right) \right] + \frac{z_{ss}}{2} \epsilon \frac{x(1 - x - \eta)}{(1 - \eta)} \quad (4)$$

where  $v_c$  is the effective volume (area in 2D) of the colloid.  $R$  is of course, measured in units of the lattice spacing. We present results for the phase behaviour of the ternary ABC model in two dimensions, using the Santos–de Haro–Yuste approximate equation of state [27] to describe the fluid phase of the hard-disk colloids. The solid phase is treated using the equation of state developed by Young and Alder [28]. We could use the same theory, to study

systems in 3D, by replacing  $F_c$  with hard-sphere equations of state and taking  $v_c$  to be the effective volume along with coordination numbers appropriate to 3D. Phase coexistence between colloidal phases I and II is computed using the following standard relations:

$$\begin{aligned} P(x_I, \eta_I) &= P(x_{II}, \eta_{II}) \\ \Delta\mu_c(x_I, \eta_I) &= \Delta\mu_c(x_{II}, \eta_{II}) \\ \Delta\mu_s(x_I, \eta_I) &= \Delta\mu_s(x_{II}, \eta_{II}) \end{aligned} \quad (5)$$

where  $P$  is the pressure,  $\Delta\mu_s = \mu_B - \mu_A$  and  $\Delta\mu_c = \mu_C - v_c\mu_A$  are chemical potentials of the solvent and colloid, respectively. The equality of temperatures in the two coexisting phases is implicit in Equation (5). The above set of equations has four unknowns, and we use an additional constraint (see appendix I of [29]). The constraint we use is  $\eta_I/(\eta_I + x_I) = c$ , where  $c$  is a constant. We start tracing the binodals at a fixed temperature by estimating a value of  $c$ , where we expect phase coexistence, and proceed to trace the entire binodal by incrementally varying  $c$ . We solve Equations (5) using Newton Raphson's method. For cases where loops occur in the phase diagram, we use the pseudo arc-length continuation technique to obtain the solution [30].

## 4. Results

### 4.1. Model parameters

In the limit  $\eta \rightarrow 0$ , the ABC model reduces to a binary (AB) solvent mixture. The solvent displays phase coexistence between an A-rich phase and a B-rich phase for temperature  $T < T_c^{\text{MF}}$ , where  $T_c^{\text{MF}}$  is the critical temperature of the binary (AB) solvent within the mean-field approximation. Due to the Ising symmetry inherent in the lattice model, the solvent phase separates at a fixed value of the chemical potential  $\Delta\mu_s = 0$ , for all  $T < T_c^{\text{MF}}$ . For  $\Delta\mu_s < 0$ , the

solvent is A-rich and for  $\Delta\mu_s > 0$ , it is B-rich in this temperature range.

We define the reduced temperature of our system as  $\tau = (T - T_c^{\text{MF}})/T_c^{\text{MF}}$ , where  $k_B T_c^{\text{MF}}/\epsilon = 1$ . All energies are scaled with the solvent-solvent interaction strength  $\epsilon$ . The two parameters of our model are  $v_c$ , which gives the size (area) of the colloid, and  $z_{cs}\alpha$  which determines the coupling strength between colloid C and solvent species B. Unless otherwise stated, we set the values of the parameters as  $v_c = 1000$  and  $z_{cs}\alpha = 32$ . In 2D for colloids of radius  $R$ ,  $v_c = \pi R^2$  is the area of a colloidal disk, and  $z_{cs} = 2\pi R$ , is the circumference of the disk. Colloids with  $\alpha > 0$  ( $\alpha < 0$ ), have a preference for species B (A), while for  $\alpha = 0$ , colloids prefer neither species. In this work, we consider a situation where the colloids prefer species B ( $\alpha > 0$ ), while the colloid-free solvent has  $\Delta\mu_s < 0$ , so that the reservoir lies on the A-rich side. We restrict our study to temperatures  $\tau > 0$ , i.e. the single phase region of the colloid-free solvent.

### 4.2. Phase behaviour in 2D

In a recent paper we investigated the phase behaviour of the ternary ABC lattice model defined by Equation (1) via Monte Carlo computer simulations [19]. In Figure 1(b) we show the phase diagram computed by simulation for colloids of radius  $R = 6$ , and a surface field  $\alpha = 0.6$ . We compare the simulation results with phase diagrams obtained from our mean-field theory in Figure 1(a). Note that for the mean-field theory we chose *empirically*  $v_c = 1000$  and  $z_{cs}\alpha = 32$ ; these values provide the best, overall qualitative agreement with the simulation results. For  $R = 6$ ,  $v_c = \pi R^2$  should be  $\simeq 113$  and  $z_{cs}\alpha \simeq 23$ . However, the hard-core repulsion of the colloids is severely underestimated by our mean-field approximation, and therefore we use a value of  $v_c$  which is very much larger. The phase diagram in Figure 1 is plotted in the  $\Delta\mu_s$  vs.  $\eta$  representation.

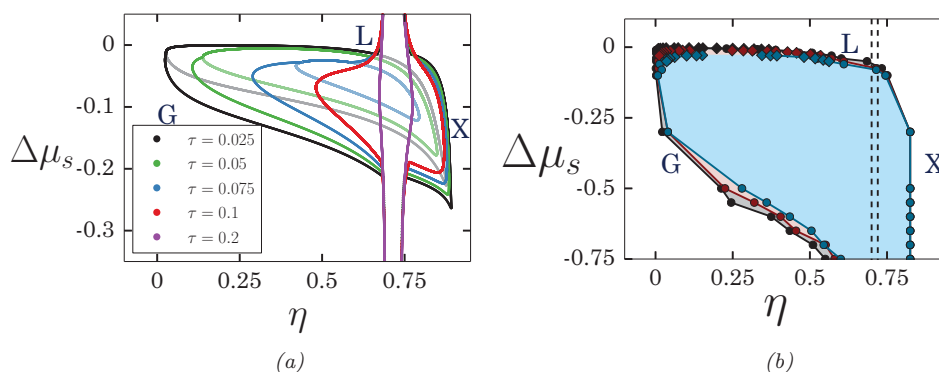


Figure 1. (a) Binodals of the ABC ternary mixture as calculated within mean-field theory for five fixed temperatures  $\tau = 0.025$  (black),  $\tau = 0.05$  (green),  $\tau = 0.075$  (blue) (these are projections of data shown in Figure 2),  $\tau = 0.1$  (red) and  $\tau = 0.2$  (purple), in the  $\Delta\mu_s$ - $\eta$  plane, i.e. solvent chemical potential vs. hard-disk (colloid) packing fraction. The grey, pale green and pale blue curves correspond to metastable colloidal G-L coexistence which terminates at a lower critical point. (b) Binodals of the same model computed with Monte Carlo simulations for three fixed temperatures  $\tau = 0.025$  (black),  $\tau = 0.05$  (dark red) and  $\tau = 0.075$  (blue) (as in figure 3(a) of [19] where  $R = 6$  and  $\alpha = 0.6$ ).

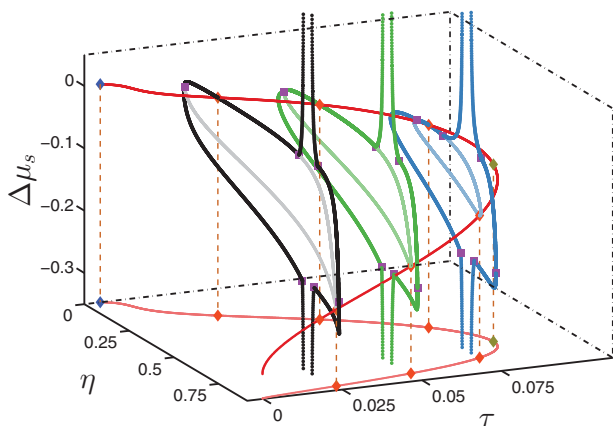


Figure 2. Binodals of the ternary ABC mixture as calculated within mean-field theory plotted in the  $\Delta\mu_s$  vs.  $\eta$  vs.  $\tau$  representation. We show slices of the full phase diagram for three fixed temperatures  $\tau = 0.025$  (black),  $\tau = 0.05$  (green) and  $\tau = 0.075$  (blue). The grey, pale green and pale blue curves correspond to metastable colloidal gas–liquid coexistence, which also terminates at a critical point. The dark red curve is the locus of critical points of the ternary mixture, this approaches smoothly the critical point of the solvent denoted by the blue diamond in the limit  $\tau \rightarrow \tau_c = 0.0$ ,  $\eta = 0$ ,  $\Delta\mu_s = 0$ . For each  $\tau$  we show the upper (stable) and lower (metastable) G-L critical points as indicated by the orange diamond symbols. The olive green diamond symbol corresponds to the point where the upper and lower critical points of the ternary system merge and disappear. The dashed orange lines (guide to the eye) connect the critical points to their projection in the  $\eta$ – $\tau$  plane. The projection of the locus of critical points in the  $\eta$ – $\tau$  plane is given by the pale red curve. The purple square symbols denote triple points. There is an upper and lower set of these – see text.

In this representation the tie lines that connect coexisting phases are horizontal, i.e. parallel to the  $\eta$  axis. Fixing  $\Delta\mu_s$ , at a fixed temperature, is equivalent to fixing the composition of the solvent reservoir. Note that the composition  $x$  of the solvent in the coexisting phases is generally very different from the composition of the solvent reservoir,  $x_r$ . It is convenient to describe the general features of the topology of the phase diagrams before comparing theory and simulation results.

In Figure 2, the two-phase or phase-coexistence region is bounded by a two-dimensional manifold (binodals) in the three-dimensional  $\eta$  vs.  $\Delta\mu_s$  vs.  $\tau$  space. Figure 1(a) displays the projections of this phase diagram in the  $\Delta\mu_s$  vs.  $\eta$  plane for different values of the reduced temperature  $\tau$ . The main features of the phase diagram are as follows: at a fixed temperature (see Figure 1), the system displays: (1) stable upper gas–liquid (G-L) coexistence and metastable lower G-L coexistence, (2) a broad gas–crystal (G-X) coexistence and (3) crystal–crystal (X-X) coexistence. The X-X coexistence that terminates at a (lower) critical point is between two phases with the same (hexagonal) structure but different lattice spacings. The upper and the metastable lower G-L coexistence curves terminate at critical points.

As the temperature increases the upper and lower critical points merge and disappear at a certain fixed temperature ( $\tau \simeq 0.0858$ ). In Figure 2 we show a red curve which is the locus of G-L critical points that originates at the critical point of the solvent reservoir ( $\eta = 0$ ,  $\tau = 0$ ,  $\Delta\mu_s = 0$ ). We also observe an upper line of G-L-X triple points and a lower line of G-X-X triple points. These are denoted by purple squares in Figure 2. The locus of the G-L-X triple points intersects the locus of critical points at  $\tau \simeq 0.077$ . This signifies the presence of a critical end point where of the three coexisting phases, a pair of phases (G-L) becomes critical. Further we observe two vertical chimneys, which approach the fluid–solid transition of hard disks in the limits  $|\Delta\mu_s| \rightarrow \infty$ . Within our present approximate treatment the fluid–solid transition is a conventional first-order freezing transition. In reality the transition is more subtle; see [31–33]. The dashed vertical lines in Figure 1(b) denote the transition region determined in [31,32].

The shapes and trends observed in the mean-field binodals upon varying temperature are consistent with simulations. In the simulations we could not confirm the presence of a lower metastable critical point, nor the presence of solid–solid coexistence. Nevertheless, it is striking that our simple mean-field theory captures the qualitative features of the phase behaviour. In Figure 1(a) we also show binodals at temperatures  $\tau = 0.1$  and  $\tau = 0.2$ . At very high temperatures, the system can display only the hard-disk fluid–solid transition. Lowering the temperature to  $\tau = 0.2$ , the fluid–solid transition region begins to broaden near  $\Delta\mu_s = 0$  (see purple curve). Upon lowering the temperature further to  $\tau = 0.1$ , the G-X transition region broadens, and the X-X transition appears (see red curve in Figure 1(a)). On further decrease of temperature the G-L coexistence appears and the two-phase regions become broader.

In Figure 3 we present the phase diagrams shown in Figure 2 in the  $x$  vs.  $\eta$  representation. As noted earlier, the composition of the solvent  $x$  is different from the composition of the solvent reservoir  $x_r$  and the tie lines in this representation are not horizontal. We show a few tie lines for the binodals at  $\tau = 0.075$  (dashed blue lines). We find that compositions of the solvent in the coexisting fluid and crystal phases are significantly different. Phase coexistence extends to regions far from the critical point of the solvent reservoir which is given by  $x_c = 0.5$  and  $\tau_c = 0$ .

#### 4.3. Locus of critical points

As can be seen from Figure 2, the critical point of the colloid-free solvent is shifted considerably upon adding a small amount of colloids. It follows that the SM interactions that arise in the ternary mixture might be very different from the universal critical Casimir interactions that pertain to a single pair of colloids, in the dilute limit  $\eta \rightarrow 0$ , when the solvent is close to its critical point. In particular the effective interactions between two colloids at state points in

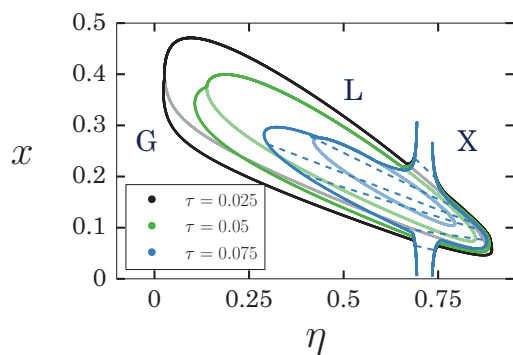


Figure 3. Binodals of the ternary ABC mixture as calculated within mean-field theory plotted in the  $x$  vs.  $\eta$  representation, i.e. the solvent composition vs. colloid fraction. We show results for three fixed temperatures  $\tau = 0.025$  (black),  $\tau = 0.05$  (green) and  $\tau = 0.075$  (blue). For the binodals at  $\tau = 0.075$ , we plot a few tie lines (dashed blue lines) that connect the coexisting phases. The grey, pale green and pale blue curves correspond to metastable G-L coexistence.

the vicinity of the critical point of the full ternary mixture will not be the same as the Casimir interactions. It is of interest to find where the critical points are located. We determine the locus of critical points using the following conditions [34]:

$$F_{cc}F_{ss} - F_{cs}^2 = 0$$

$$F_{sss}F_{cc}^2 - F_{ccc}F_{ss}F_{cs} - 3F_{css}F_{cc}F_{cs} + 3F_{ccs}F_{cc}F_{ss} = 0$$

Here the subscripts  $s$  and  $c$  denote partial differentiation of the Helmholtz free energy  $F$ , with respect to the number of solvent ( $N_s$ ) and colloidal particles ( $N_c$ ), respectively. In Figure 4 we show the locus of critical points, together with the phase diagram of the solvent reservoir, for two different systems. In the inset of Figure 4 we show the approach of the loci of critical points to the critical point of the solvent reservoir. For  $z_{cs}\alpha = 24$ , the locus of critical points approaches monotonically the critical point of the solvent

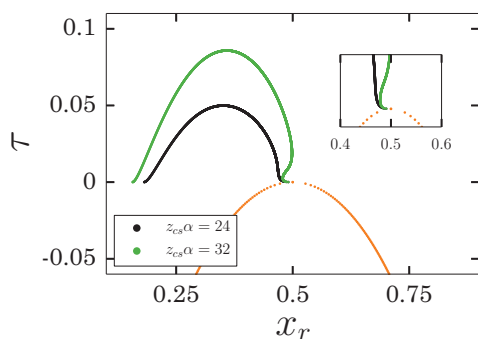


Figure 4. Loci of gas-liquid critical points for ternary ABC mixtures with  $v_c = 1000$ , and two different values of  $z_{cs}\alpha$ . The inset shows the behaviour of the loci close to the critical point of the solvent reservoir  $x_r = x_c = 0.5$ ,  $\tau = 0$ . The dotted orange line is the binodal of the colloid-free AB solvent.

reservoir ( $\tau = 0$ ,  $x_r = 0.5$ ). By contrast, for  $z_{cs}\alpha = 32$ , there is a non-monotonic dependence on the composition of the solvent reservoir. Note that increasing the coupling strength  $z_{cs}\alpha$  shifts the maximum in the line of critical points to higher  $\tau$ , but does not change the composition at the maximum.

#### 4.4. Aggregation lines

Typically experiments on colloidal aggregation [13,17] are performed by suspending a fixed number of colloids in a solvent at a fixed solvent composition  $x_r$ . The temperature of the system is then adjusted to (reversibly) induce aggregation. At fixed  $\eta$  and  $x_r$ , the locus of points at which aggregation is first observed is called an aggregation line; for an experimental measurement see figure 3 in [13]. We compute the aggregation line as follows. Draw a vertical line at say  $\eta = 0.1$  in Figure 1. This intersects the binodal for say,  $\tau = 0.025$  at solvent chemical potentials  $\Delta\mu_s^I$  and  $\Delta\mu_s^{II}$ , corresponding to solvent reservoir compositions  $x_r^I$  and  $x_r^{II}$ . Begin at  $x_r^I$ , change the temperature infinitesimally, and travel along the manifold of coexisting states, at fixed  $\eta$ . Thus at  $\tau + \delta\tau$ , we obtain a new value of solvent reservoir composition. The locus of such points plotted in the  $\tau$  vs.  $x_r$  representation gives the aggregation line. This line serves to demarcate the one-phase region, which lies outside the lines, and the region inside where phase separation can be found. In other words, given a suspension with a fixed packing fraction  $\eta$  of colloids, with the solvent composition fixed, a point on the aggregation line at  $x_r$  gives the temperature at which aggregates may be first observed upon cooling the suspension. Note that on adding a small amount of colloids, the critical point of the ternary mixture shifts from that of the solvent reservoir and therefore the aggregation lines terminate before reaching  $\tau = 0$ ,  $x_r = x_c = 0.5$ .

In Figure 5 we show our mean-field result for the aggregation lines at fixed colloid packing fractions of  $\eta = 0.1$  and  $\eta = 0.05$ . Here  $v_c = 1000$ , and  $z_{cs}\alpha = 32$  are the same as in Figures 1(a), (2) and (3). For these sets of parameters, the aggregation lines reside on the A-rich region of the phase diagram,  $x_r < 0.5$  and upon increasing the packing fraction  $\eta$ , aggregation lines are shifted to higher temperatures. Note that these lines extend to the subcritical region of the colloid-free solvent,  $\tau < 0$ . However, in this regime we can expect capillary bridging between colloids to occur and our simple mean-field description, based solely on excluded volume considerations, is not expected to account for this.

In Figure 6(a) and 6(b) we show projections of the phase diagram (Figure 2) in the  $\tau$  vs.  $\eta$  plane, i.e. we fix the value of the composition of the solvent reservoir  $x_r$  and thus the ratio  $\Delta\mu_s/k_B T$ . In Figure 6(a) projections are plotted at two values of the solvent reservoir composition:  $x_r = 0.495$  (green curves) and  $x_r = 0.41$  (blue curves). For the first

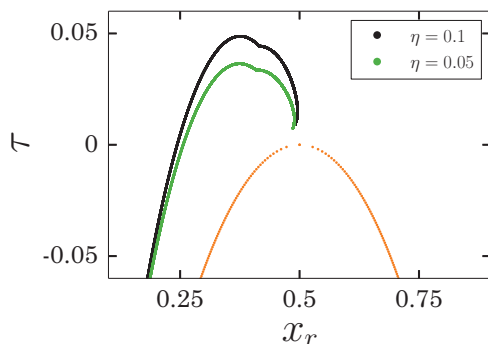


Figure 5. Aggregation lines for a ternary ABC mixture with  $v_c = 1000$ ,  $z_{cs}\alpha = 32$ , at two fixed values of colloid packing fraction:  $\eta = 0.1$  and  $\eta = 0.05$ . The dotted orange line is the binodal of the colloid-free AB solvent. Note that the aggregation lines terminate at points removed from the critical point of the solvent reservoir – see text.

composition, with  $x_r$  close to the critical composition  $x_c = 0.5$ , we observe a tiny G-L phase coexistence region, located at small values of  $\tau$ . At the second composition, further away from  $x_c$ , the phase coexistence region broadens (blue curves), with the G-L coexistence becoming metastable at sufficiently high  $\tau$ , with respect to a broad gas–crystal (G-X) coexistence. In Figure 6(b) we plot the projections for a solvent composition of  $x_r = 0.418$ . For this composition, on reducing  $\tau$  we first see a G-L coexistence (blue curve) region near  $\tau = 0.075$ . Reducing  $\tau$  further we see a G-X coexistence (green curve) region between about  $\tau = 0.07$  and  $0.05$ , and for even lower values of  $\tau$ , G-L coexistence (blue curve) becomes stable again.

#### 4.5. Dependence of phase behaviour on adsorption strength $z_{cs}\alpha$

Here we investigate the dependence of the phase behaviour on  $\alpha$ , the coupling strength or wettability of the colloids.

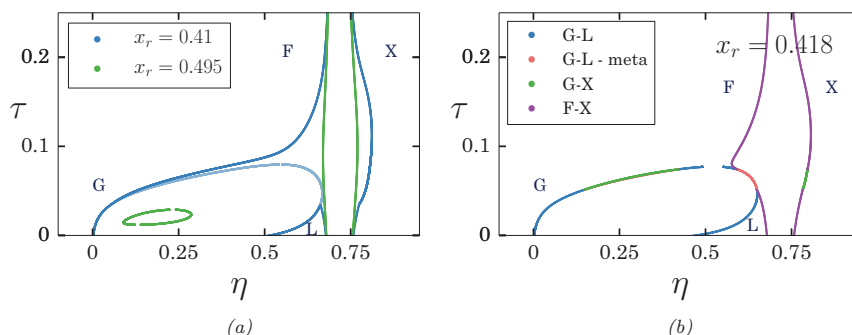


Figure 6. (a) Phase diagram of the ternary ABC mixture for  $v_c = 1000$ ,  $z_{cs}\alpha = 32$ , at temperature  $\tau = 0.025$ , for two different fixed compositions of the solvent reservoir:  $x_r = 0.495$  (green curves) and  $x_r = 0.41$  (blue curves) in the temperature  $\tau$  vs. colloid packing fraction  $\eta$  representation. The pale blue curve corresponds to metastable G-L coexistence. (b) Same as (a), except for the solvent composition  $x_r = 0.418$ . The blue, green and purple curves correspond to G-L, G-X and F-X coexistence, respectively. The red curve indicates metastable G-L coexistence.

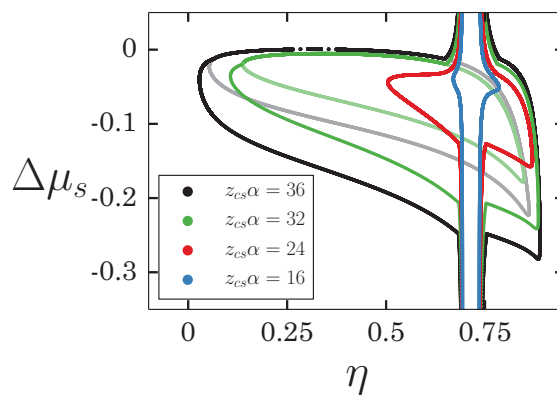


Figure 7. Phase behaviour of the ternary ABC mixture at temperature  $\tau = 0.05$ , for  $z_{cs}\alpha = 36$  (black curve),  $z_{cs}\alpha = 32$  (green curve),  $z_{cs}\alpha = 24$  (red curve) and  $z_{cs}\alpha = 16$  (blue curve) in the solvent chemical potential  $\Delta\mu_s$  vs. colloid packing fraction  $\eta$  representation. The grey and pale green curves correspond to metastable G-L coexistence.

For  $\alpha = 0$ , the colloid prefers neither species of the solvent. As  $\alpha$  increases, the preference of colloids for species B increases, and this drives phase separation to  $\Delta\mu_s < 0$ . In Figure 7, we fix  $v_c = 1000$ ,  $z_{cs} = 40$  and  $\tau = 0.05$ , and present the binodals for several values of  $\alpha$ . With increasing  $\alpha$  first G-X coexistence appears and expands for  $\Delta\mu_s \simeq 0$  (see blue and red curves). Upon further increasing  $\alpha$ , the gas–liquid coexistence appears and broadens (see green and black curves). The trend observed is similar to the change in phase behaviour found upon changing temperature for fixed  $v_c$  and  $z_{cs}\alpha$  (see Figure 1(a)). However, we find for  $z_{cs}\alpha = 36$  (black curve) the G-L envelope extends slightly into the region  $\Delta\mu_s \geq 0$ . As mentioned earlier, for chemical potentials  $\Delta\mu_s > 0$ , the bulk solvent reservoir is B-rich and the colloids prefer the same species B. There appears to be no incentive for phase separation under these conditions, and therefore these predictions of the theory are somewhat

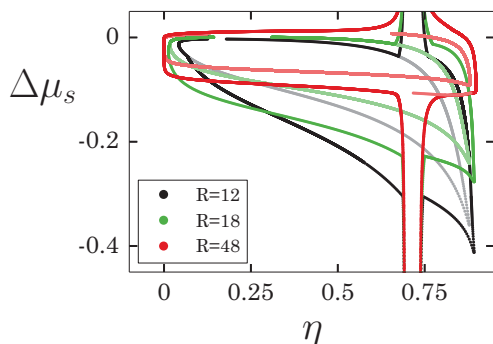


Figure 8. Phase behaviour of the ternary ABC mixture at temperature  $\tau = 0.025$ , for colloid radius  $R = 12$  (black curve),  $R = 18$  (green curve),  $R = 48$  (red curve), in the solvent chemical potential  $\Delta\mu_s$  vs. colloid packing fraction  $\eta$  representation.  $\alpha = 0.3$  is fixed – see text. The grey and pale green curves correspond to metastable G-L coexistence; these terminate at lower critical points. The two pale red curves correspond to metastable G-L and metastable X-X coexistence, respectively.

puzzling. Furthermore, in simulations we observed that for  $\Delta\mu_s \geq 0$ , the colloids always stay solvated by species B.

#### 4.6. Dependence of phase behaviour on colloid radius $R$

Finally we study the dependence of the phase behaviour of the ternary ABC mixture on the size of the colloid. We fix  $\tau = 0.025$ ,  $\alpha = 0.3$  and compute the binodals for three different radii  $R$  of the colloid. More precisely, the parameters here are given by  $v_c = \pi R^2$ ,  $z_{cs} = 2\pi R$ . The resulting mean-field binodals are shown in Figure 8. Upon increasing  $R$ , the G-L and G-X coexistence regions broaden. However, these also terminate, or merge with the hard-disk mean-field fluid–solid transition, at higher values of  $\Delta\mu_s$ . The features of the binodals for  $R = 12$  and  $R = 18$  are very similar to those reported in detail for  $v_c = 1000$  and  $z_{cs}\alpha = 32$  in Figure 1(a). Upon increasing the radius to  $R = 48$ , both the gas–liquid and crystal–crystal transitions become metastable with respect to the broad gas–crystal transition. Once again it is intriguing that for radius  $R = 48$  the G-X and the metastable G-L binodals extend beyond  $\Delta\mu_s \geq 0$ . We suggest this is an artefact of our crude mean-field treatment.

## 5. Summary and conclusions

The results presented here show that the mean-field theory, crude as it is, captures all the qualitative features of the phase diagram of the lattice model, defined by Equation (1), found in the simulations [19]. We summarise the main features.

- (1) The theory predicts rich colloidal phase behaviour. In addition to the fluid–solid transition of the bare

hard-disk colloids, incorporated into the theory via the pure colloid free energy  $F_c(\eta, T)$ , the theory predicts upper stable gas–liquid (G-L), lower metastable G-L coexistence, gas–crystal (G-X) and crystal–crystal (X-X) phase coexistence.

- (2) Gas–liquid coexistence curves, calculated for fixed temperature, terminate at upper and lower critical points. The locus of such critical points approaches the critical point of the solvent reservoir in the limit  $\eta \rightarrow 0$ ,  $\tau \rightarrow 0$ ,  $\Delta\mu_s \rightarrow 0$  – see Figure 2. The precise shape of the locus of critical points in this limit depends on  $z_{cs}\alpha$ , the value of the coupling strength between the colloid and the solvent – see Figure 4.
- (3) The critical point of the ternary mixture can be shifted far from that of the colloid-free solvent when only small amounts of colloid are added.
- (4) It is clear from Figure 3 that the composition of the solvent in the two coexisting colloidal phases is very different. Any successful effective one-component approach must be able to describe this fractionation.
- (5) Key results of our study are the aggregation lines presented in Figure 5. These resemble qualitatively the experimental results of Beysens [13] referred to in the Introduction. The aggregation lines are present in the A-rich region of the phase diagram,  $x_r < x_c$  as expected, and terminate very close to the critical composition  $x_c$  of the solvent. We return to this below.
- (6) We studied the dependence of the phase behaviour on colloid size and adsorption strength (wettability) – see Figures 7 and 8. No new features appeared in the topology of the phase diagrams. However, for large values of the coupling strength  $z_{cs}\alpha$  at fixed radius  $R$  and large values of  $R$  at fixed  $z_{cs}\alpha$ , the colloidal G-L coexistence extends to  $\Delta\mu_s > 0$ , i.e. very slightly into the B-rich region of the solvent phase diagram. This could be an artefact of our mean-field approach.
- (7) We have performed a few calculations in  $D = 3$  using the same form of free-energy (Equation (4)) but with the equations of state appropriate to hard spheres [35,36]. The topology of the mean-field phase diagrams is unaltered from  $D = 2$  but the detailed shape and numerical values depend strongly on the parameters  $R$  and  $\alpha z_{cs}$ . Given our theory is a mean-field one, this is not surprising!

In drawing conclusions from our study we must recognise that most of the results presented are for an empirical choice of parameters:  $v_c = 1000$  and  $z_{cs}\alpha = 32$ . These do not correspond to the actual values of  $R$  and  $\alpha$  set by the underlying Hamiltonian equation (1), and therefore, those values used in the simulations. Our aim was rather to ask whether a physical choice would yield phase diagrams that

are overall similar to those of the simulations and then investigate the underlying details of the phase behaviour. Clearly our mean-field treatment allows us to do this and to investigate the trends in phase behaviour that could be expected on changing  $R$  and  $\alpha$ . Recognising our approach is mean-field and therefore cannot capture properly the effects of fluctuations, particularly strong in  $D = 2$ , we cannot hope to do better.

Finally we return to aggregation lines. Part of the motivation for our study was to re-address the origin of the aggregation lines found in experiment. We take the view that aggregation corresponds to the onset of colloidal phase separation in the full ternary mixture, as is represented in Figure 5. The shape of our aggregation lines is similar to those found in the original experimental study of Beysens and Estève [13] – see their figure 3. Of course one must transcribe to their system of silica colloids in a WL solvent which has a *lower* critical point. Our model has an upper critical point. Making the appropriate transcription one finds that the aggregation lines found in the present treatment lie on the appropriate side of coexistence and curve towards the solvent critical point, see figures 3 and 5(b) of [13] – in the same way as the experimental lines.

It is probably not appropriate to attempt quantitative comparisons. We should bear in mind that the length scales studied in theory and in the simulations [19] are rather different from those pertinent to the experiments. For example, in [13] the packing fraction of the silica colloids is very small and the aggregation line lies  $\sim 0.4$  K below the solvent binodal. This corresponds to  $\tau \sim 1.3 \times 10^{-3}$  and the ratio of correlation length to colloid radius,  $\xi/R$ , is about 0.2. By contrast, if we consider Figure 5 and take  $\tau \sim 0.03$  this ratio is about 3. It is also interesting to consider the recent experiments of Nguyen *et al.* [17], who investigate poly-*n*-isopropyl acrylamide (PNIPAM) particles in a quasi two-component solvent consisting of 3-methyl pyridine, water and heavy water; the packing fraction of the particles is  $\sim 0.02$ . Aggregation is first observed on heating to 0.3 K below the solvent (lower) critical temperature, corresponding to  $\tau \sim 0.9 \times 10^{-4}$  and  $\xi/R$  is about 0.2. In [17] liquid-like aggregates are first observed. On raising the temperature by a further 0.1 K the particles inside the aggregates form an fcc crystal. We can ask whether this scenario is found in our theory. In Figure 6(a) we find for  $x_r = 0.41$  lowering the temperature towards the solvent critical temperature yields first G-X coexistence which is followed by G-L coexistence for  $\tau \lesssim 0.025$ . For a slightly different solvent composition  $x_r = 0.418$ , see Figure 6(b), we observe G-L coexistence followed by G-X coexistence as in [17]. However, on lowering  $\tau$  even further we find stable G-L coexistence; this is not reported in [17]. Our study points to the wide variety of phase behaviour that might occur in systems of this type. Indeed it suggests that nanoparticles immersed in a binary solvent near criticality might exhibit very rich phase diagrams and aggregation phenomena.

## Acknowledgements

It is a great pleasure to contribute to this Special Issue in honour of Jean-Pierre Hansen. R. Evans first met Jean-Pierre in 1977 in Corsica, Corsica; we were both teaching at a NATO Summer School on liquids. Jean-Pierre's lectures on 'correlation functions and their relationship with experiments', delivered with his trademark gusto and clarity at a small chalkboard, made a lasting impression on all who attended. This included the escapee from the nearby penitentiary who quickly decided he should give himself up. Jean-Pierre's seminars, research articles, reviews and, in particular, his books have been a continuous source of inspiration for R. Evans and countless others in our field. M. Dijkstra and R. van Roij first met Jean-Pierre in the early 1990s during a three-month work visit (M. Dijkstra) to 'his' Laboratoire de Physique at the Ecole Normale Supérieure in Lyon, France, and later at a NATO school on phase transitions in complex fluids in Varenna, Italy. Jean-Pierre's immense knowledge on any aspect of liquids and soft matter has impressed us ever since. M. Dijkstra and R. van Roij still benefit from the excellent scientific guidance Jean-Pierre offered to us when we were young postdocs in Oxford (1995) and Lyon (1997), respectively. Jean-Pierre's handwritten manuscripts (without any erasements) and the unimaginably broad content of 'The Book' (which keeps revealing new details with every read), as well as his charming personality, his broad interest in architecture, paintings and politics, and the exquisite dinner parties in Trambly and Oxford, are but a few of the lasting impressions he made on us. We wish Jean-Pierre and Martine all the very best in the coming years.

## Disclosure statement

No potential conflict of interest was reported by the authors.

## Funding

J.R. Edison and M. Dijkstra acknowledge financial support from a Nederlandse Organisatie voor Wetenschappelijk Onderzoek (NWO) VICI grant.

## References

- [1] G. Flöter and S. Dietrich, *Z. Phys. B* **97**, 213 (1995).
- [2] M.E. Fisher and P.G. de Gennes, *C. R. Acad. Sci. Paris B* **287**, 207 (1978).
- [3] C. Hertlein, L. Helden, A. Gambassi, S. Dietrich, and C. Bechinger, *Nature* **451**, 172 (2008).
- [4] A. Gambassi, A. Maciołek, C. Hertlein, U. Nellen, L. Helden, C. Bechinger, and S. Dietrich, *Phys. Rev. E* **80**, 061143 (2009).
- [5] M. Krech, *The Casimir Effect in Critical Systems* (World Scientific, Singapore, 1994).
- [6] O. Vasilyev, A. Gambassi, A. Maciołek, and S. Dietrich, *Phys. Rev. E* **79**, 041142 (2009).
- [7] H.T. Dobbs, G.A. Darbellay, and J.M. Yeomans, *Europhys. Lett.* **18**, 439 (1992).
- [8] C. Bauer, T. Bieker, and S. Dietrich, *Phys. Rev. E* **62**, 5324 (2000).
- [9] P. Hopkins, A.J. Archer, and R. Evans, *J. Chem. Phys.* **131**, 124704 (2009).
- [10] R. Okamoto and A. Onuki, *Phys. Rev. E* **88**, 022309 (2013).
- [11] P.J. Upton, J.O. Indekeu, and J.M. Yeomans, *Phys. Rev. B* **40**, 666 (1989).
- [12] A.J. Archer, R. Evans, R. Roth, and M. Oettel, *J. Chem. Phys.* **122**(8), 084513 (2005).

- [13] D. Beysens and D. Estève, *Phys. Rev. Lett.* **54**, 2123 (1985).
- [14] Y. Jayalakshmi and E.W. Kaler, *Phys. Rev. Lett.* **78**, 1379 (1997).
- [15] H. Guo, T. Narayanan, M. Sztuchi, P. Schall, and G.H. Wegdam, *Phys. Rev. Lett.* **100**, 188303 (2008).
- [16] D. Bonn, J. Otwinowski, S. Sacanna, H. Guo, G. Wegdam, and P. Schall, *Phys. Rev. Lett.* **103**, 156101 (2009).
- [17] V.D. Nguyen, S. Faber, Z. Hu, G.H. Wegdam, and P. Schall, *Nat. Commun.* **4**, 1584 (2013).
- [18] D. Beysens and T. Narayanan, *J. Stat. Phys.* **95**, 997 (1999).
- [19] J.R. Edison, N. Tasios, S. Belli, R. Evans, R. van Roij, and M. Dijkstra, *Phys. Rev. Lett.* **114**, 038301 (2015).
- [20] H. Löwen, *Phys. Rev. Lett.* **74**, 1028 (1995).
- [21] T. Gil, J. H. Ipsen, and C.F. Tejero, *Phys. Rev. E* **57**, 3123 (1998).
- [22] T.J. Sluckin, *Phys. Rev. A* **41**, 960 (1990).
- [23] T.F. Mohry, A. Maciołek, and S. Dietrich, *J. Chem. Phys.* **136**, 224903 (2012).
- [24] T.F. Mohry, A. Maciołek, and S. Dietrich, *J. Chem. Phys.* **136**, 224902 (2012).
- [25] T.F. Mohry, S. Kondrat, A. Maciołek, and S. Dietrich, *Soft Matter* **10**, 5510 (2014).
- [26] M.T. Dang, A.V. Verde, V.D. Nguyen, P.G. Bolhuis, and P. Schall, *J. Chem. Phys.* **139**(9), 094903 (2013).
- [27] A. Santos, M. López de Haro, and S. Bravo Yuste, *J. Chem. Phys.* **103**(11), 4622 (1995).
- [28] D.A. Young and B.J. Alder, *J. Chem. Phys.* **70**, 473 (1979).
- [29] J. Köfinger, N.B. Wilding, and G. Kahl, *J. Chem. Phys.* **125**, 234503 (2006).
- [30] H.B. Keller, in *Applications of Bifurcation Theory*, edited by P.H. Rabinowitz (Academic Press, New York, 1977), pp. 359–384.
- [31] E.P. Bernard and W. Krauth, *Phys. Rev. Lett.* **107**, 155704 (2011).
- [32] M. Engel, J.A. Anderson, S.C. Glotzer, M. Isobe, E.P. Bernard, and W. Krauth, *Phys. Rev. E* **87**, 042134 (2013).
- [33] W. Qi, A.P. Gantapara, and M. Dijkstra, *Soft Matter* **10**, 5449 (2014).
- [34] S. Chatterjee and P.G. Debenedetti, *J. Chem. Phys.* **124**, 154503 (2006).
- [35] N.F. Carnahan and K.E. Starling, *J. Chem. Phys.* **51**, 635 (1969).
- [36] R.J. Speedy, *J. Phys. Condens. Matter* **10**, 4387 (1998).